A study on the influence of internal structures on the shape of pyroclastic particles by X-ray microtomography investigations

Daniela Mele[1], Fabio Dioguardi[2], Pierfrancesco Dellino[1]

[1]Dipartimento di Scienze della Terra e Geoambientali, Università degli Studi di Bari "Aldo Moro", via E. Orabona 4, 70125 Bari, Italy

[2] British Geological Survey, The Lyell Centre, Research Avenue South, Edinburgh EH14 4AP, UK

Corresponding author:

Mele Daniela,

daniela.mele@uniba.it

Dipartimento di Scienze della Terra e Geoambientali (Università degli Studi di Bari "Aldo Moro"

Via E. Orabona 4, 70125 Bari

Phone number: +393470669670

Co-authors:

Fabio Dioguardi: fabiod@bgs.ac.uk; British Geological Survey, The Lyell Centre, Research Avenue South, Edinburgh EH14 4AP, UK

Pierfrancesco Dellino: pierfrancesco.dellino@uniba.it; Dipartimento di Scienze della Terra e Geoambientali, Università degli Studi di Bari "Aldo Moro", via E. Orabona 4, 70125 Bari, Italy

Sector: Volcano physics

Type of material submitted: Research Article

Abstract

X-Ray computed microtomography is a non-destructive 3D imaging technique that can be used for the investigation of both the morphology and internal structures of a solid object. Thanks to its versatility, it is currently of common use in many research fields and applications, from medical science to geosciences. The latter includes volcanology, where this analytical technique is becoming increasingly popular, in particular for quantifying the shape as well as the internal structure of particles constituting tephra deposits. Particle morphology plays a major role in controlling the mobility of pyroclastic material in the atmosphere and particle-laden flows, while the internal

structure (e.g. vesicles and crystal content) is of importance in constraining the processes that occurred in magmatic chambers or volcanic conduits.
In this paper, we present results of X-Ray microtomography morphological and textural analyses on volcanic particles carried out to study how particle shape is influenced by internal structures. Particles were selected from tephra generated during explosive eruptions of different magnitudes and compositions. Results show that particle morphology is strongly influenced by internal structure, which is characterized by textural features like vesicularity, vesicle and solid structure distribution, vesicle inter-connectivity and distance between adjacent vesicles. These have been found to vary with magma composition, vesiculation and crystallization history. Furthermore, our results confirm that X-Ray microtomography is a powerful tool for investigating shape and internal structure of particles. It allows us to both characterize the particle shape by means of tridimensional shape parameters and relate them to their internal structures.

Key words: 3D sphericity, 3D fractal dimension, volcanic particles, particle shape, microtomography, textural properties, vesicularity.

1. INTRODUCTION

During explosive eruptions, particles of variable size, shape and density are injected into the atmosphere and, depending on the eruptive size and style, can have an impact on human beings, infrastructure and activities from local up to global scale [Blong, 1984; Casadevall 1994; Horwell and Baxter, 2006; Bonadonna et al., 2012; Wilson et al. 2012, 2014; Beckett et al., 2015]. The physical properties of pyroclastic particles (size, shape, density) affect their aerodynamic behavior, i.e. the aerodynamic drag force. Many studies have been carried out over the past few decades focusing on the dependency of the aerodynamic drag on particle shape, especially in the field of multiphase flow dynamics [Sneed and Folk, 1958; Wilson and Huang, 1979; Haider and Levenspiel, 1989; Swamee and Ojha 1991; Ganser 1993; Rodrigue et al., 1994; Chien 1994; Taylor, 2002; Tran-Cong et al., 2004; Dellino et al., 2005; Pfeiffer et al. 2005; Loth; 2008; Hölzer and Sommerfeld, 2008; Mele et al., 2011; Dioguardi and Mele, 2015; Bagheri and Bonadonna, 2016; Dioguardi et al., 2017, 2018]. In these studies, several shape-dependent drag laws have been proposed, which depend on one or more shape descriptors that are generally functions of 1D and 2D parameters. More recently, the use of X-Ray microtomography (μX-CT) has enabled improvements in the ability to investigate the internal structures and morphologies of materials with a non-destructive and three-dimensional (3D) visualization and quantification [Song et al., 2001; Ersoy et al., 2010; Voltolini et al., 2011; Baker et al., 2012; Cnudde and Boone, 2013; Rausch et al., 2015; Vonlanthen et al. 2015; Bagheri et al., 2015; Polacci et al., 2018]. In particular, 3D shape descriptors quantified by means of μX-CT analyses have been introduced and applied to predict the aerodynamic drag of volcanic particles [e.g. Dioguardi et al. 2017].

Recently, Mele and Dioguardi [2018] presented a study on the dependency of particle shape on the size of vesiculated volcanic juvenile particles analyzed with μX-CT. The study proved how the shape of these particles, which are commonly generated during explosive eruptions fed by evolved vesiculated magmas, is the result of the interaction between particle size and the size distribution of vesicles. This means that the general assumption made when simulating the transport of volcanic ash in the atmosphere by means of dispersion models [e.g. Costa et al. 2006; Jones et al., 2007; Mastin et al., 2013], i.e. assuming a size-independent particle shape, does not hold for these types of eruptions. This is the assumption made, for example, by London VAAC when using the standard grainsize distribution for operational forecasts [see Beckett et al. 2015]. Particle shape plays a crucial role in the multiphase flows occurring on Earth's surface, including sandstorms [e.g. Kok et al., 2012, Doronzo et al. 2015] and turbulent density currents [e.g. Branney and Kokelaar, 2002; Dufek, 2016; Dioguardi and Mele, 2018; Dellino et al. 2018]. In fact, Dioguardi et al. [2014] showed how implementing shape-dependent drag parametrizations into multiphase computational fluid dynamic models improve their performance in predicting the particle trajectories and fall velocity.

With the aim of further investigating the dependency of particle shape on the internal texture of volcanic particles, we carried out a systematic quantification of different internal textural properties of volcanic particles collected from tephra fallout deposits of eruptions of different magnitudes, styles and magma composition. In this paper, we first describe particle samples and the employed technique, and then we present results of the analysis on the relationship between particle morphology and internal structural characteristics, namely the fraction of vesicles and how these are inter-connected and/or distributed.

2. MATERIALS AND METHOD

In order to investigate the influence of internal texture on particle shape, we used the same set of juvenile particles employed in Dioguardi et al. [2017]. The samples were from the juvenile component of fallout deposits emplaced by the following eruptions: 1) Eyjafjallajökull 2010 [Dellino et al., 2012] and Grímsvötn 2004 [Jude-Eton et al., 2012], eruptions of trachybasalt and basaltic composition in Iceland, respectively; 2) Mt. Etna 2001 [Scollo et al., 2007], of basaltic composition (trachybasalt); 3) Pomici di Avellino Plinian eruption of Vesuvius (3900 BP; Sulpizio et al., 2010), of tephritic-phonolitic composition; 4) AD 472 (Pollena) sub-Plinian eruption of Vesuvius [Sulpizio et al., 2005] of tephritic-phonolitic composition; 5) Agnano Monte-Spina Plinian eruption of Campi Flegrei (4500 BP; de Vita et al., 1999), of trachytic composition. In this work, all particles were generated during explosive eruptions driven by dry magmatic fragmentation [Dellino et al., 2001; Sulpizio et al., 2005; Scollo et al., 2007; Sulpizio et al., 2010; Dellino et al., 2012], with the exception of particles from the Grímsvötn 2004 eruption, which were the product of magma-water interaction [Jude-Eton et al., 2012].

We used particles of the same grain-size interval, i.e. 0.500-0.355 mm because, as shown in Mele et al. [2011] and Mele and Dioguardi [2018], they have a more irregular contour, including a significant number of vesicles on the particle surface.

For each sample suite, the 3D external morphology and internal texture of 15 particles were reconstructed by means of μX-CT imaging with a Bruker Skyscan 1172 high-resolution μX-CT scanner. Particles were cleaned in an ultrasonic bath and mounted on a graphite rod holder using vinyl glue. The parameters used for the acquisition of μX-CT radiograph are shown in Table 1. In order to detect vesicles across the widest possible range of sizes, particles were scanned with a pixel size of 1.02 μm, which, as shown in Mele and Dioguardi [2018], is enough to sample the fine vesicle population.

Bruker's NRecon software [Liu and Sasov, 2005] was used to reconstruct μX-CT projection images into two-dimensional cross sections (slices) by applying the Feldkamp algorithm [Feldkamp et al., 1984]. Cross-section reconstruction parameters are shown in Table 1.

3D quantitative image analysis of shape and internal textures of particles was performed using Bruker's CTAn software [Skyscan, 2009]. Each particle was segmented from the background (holder, glue and air) using a global threshold [Otsu, 1979]. It is to be noted that by internal texture we mean both vesicles and the solid structure. The latter is represented by both glass and crystals due to the difficulty of discriminating between these two components using the microtomographic technique since, in most cases, they have a similar X-Ray attenuation coefficient [Arzilli et al. 2016].

To quantify particle shape, the sphericity Φ_{3D} and Fractal dimension D_{3D} [Dioguardi et al. 2017] were calculated.

Sphericity is defined by:

$$\Phi_{3D} = \frac{A_{sph}}{A_p} = \frac{\sqrt[3]{(6V_p)^{\frac{2}{3}}}}{A_p} \quad (1)$$

where A_{sph} is the surface area of the sphere equivalent to the particle of volume V_p and A_p is the particle surface area. The calculation of particle volume, i.e. the number of voxels of the binarised solid object times the volume of one voxel, is carried out by means of the hexahedral marching cubes volume model [Lorensen and Cline, 1987]. The 3D particle surface area calculation is based on the faceted surface of the marching cubes volume model [Lorensen and Cline, 1987]. By definition, Φ_{3D} ranges between 0 and 1, being 1 the value of a perfect sphere.

Fractal dimension (D_{3D}) is defined by:

$$L = ks^{-D_{3D}} \quad (2)$$

where L is the length of the fractal line approximating the contour of the object with ever-decreasing segments of length scale s, D_{3D} is the fractal dimension and k is a number. Graphically D_{3D} is the slope of the line in the plot log(L) vs. log(s). D_{3D} was calculated by an algorithm based on the "box counting" method [Chappard et al., 2001], by which the 3D digital object is approximated by an array of equal-sized cubes, which are counted. The procedure is repeated over a range of cube sizes, and the number of cubes is plotted against cube size in a log-log plot. D_{3D} is the slope of the regression line. D_{3D} is equal to 2 for a sphere. The more D_{3D} is larger than 2, the more a particle is irregular in shape

As far as the internal structure analysis is concerned, for each particle a Volume of Interest (VOI) with the same shape of particle without vesicles was created by a shrink-wrap operation (Figure 1). The latter was necessary in order to investigate the total size-range of vesicles inside particles.

The following parameters were then evaluated: vesicularity, vesicle-size distribution, solid structure distribution, surface convexity index of vesicles and structure linear density of vesicles.

Vesicularity (%) is defined as the fraction of the total volume of a sample occupied by vesicles or voids, encompassing open and closed vesicles, i.e. the volume of all open plus closed pores as percent of the total VOI volume.

Vesicle-size or solid structure distribution (mm) are the fractions of vesicle or solid structure volume that are within a specific range of vesicle size. Its calculation involves two steps: skeletonisation, which identifies the medial axes of all vesicles or solid structures, and sphere-fitting that measures the local thickness for all the voxels lying along this axis [Remy and Thiel, 2002]. The average diameter and standard deviation of vesicle and solid structure size distribution were also calculated.

Surface convexity index of vesicles (mm^{-1}), also known as Fragmentation index, is characterized by the rupture of connectivity [Hahn et al., 1992; Promentilla et al. 2009]. It is calculated by comparing volume and surface of binarised vesicles before and after a single voxel image dilation, i.e.

$$FI = \frac{S_1 - S_2}{V_1 - V_2} \quad (3)$$

where S and V are vesicle surface and volume and the subscript numbers 1 and 2 mean before and after image dilation. The more negative the surface convexity index is, the greater is the vesicle connectivity.

Structure linear density of vesicles (mm^{-1}), also known in medical sciences as the trabecular number, is the number of vesicles per unit length on a linear path through the structure, given by the inverse of the mean distance between the medial axes of the vesicle structure [Hildebrand et al., 1999]. High structure linear density value means that the thickness of solid structure, which separates vesicles, is small; i.e. vesicles are very close together.

3. RESULTS

The averages and standard deviations of all the measured parameters are listed in Table 2; Figure 2 shows the typical morphologies of representative particles chosen from each sample suite illustrated by 3D volume rendering. Data show that the Avellino and Grímsvötn particles represent the two end-members of both vesicularity and particle shape measured ranges. Grímsvötn particles display the lowermost vesicularity and the highest sphericity and the lowermost fractal dimensions (Table 2) whereas particles sampled from the Avellino eruption deposits are the most irregular of the analyzed samples.

We then determined the vesicle size distribution of all the particles of every sample suite; the distributions are shown in Figure 3. Two different groups can be clearly discerned by a simple first qualitative analysis of the vesicle size distribution: Avellino, Pollena and Agnano Monte Spina on one side (Group 1), Eyjafjallajökull, Grímsvötn and Etna particles on the other (Group 2). Group 1 particles show a finer vesicle population and a narrower distribution than particles of Group 2. Interestingly, samples from eruptions of similar composition tend to group together: Group 1 include samples of eruptions fed by tephritic-phonolitic and trachytic vesiculated magmas; Group 2 is made by particles from basaltic and trachybasaltic eruptions. A similar trend can be inferred from the plots of the solid structure distribution (Figure 3). Particles from Group 1 are characterized by a thinner solid structure than basaltic and trachybasaltic particles, which on the contrary show a very variable thickness of the solid structure (Figure 3). Comparing the average size of both vesicles and solid structures (Figure 2), we can observe that particles of Group 1 are characterized by both smaller vesicles and a less thick solid structure than basaltic particles (Group 2), although few particles of Avellino, Pollena and Agnano Monte Spina eruptions have a thick solid structure. This can be attributed to:

- the presence of large phenocrysts (Figure 2), which are characterized by a solid structure histogram with a different population (for example grey and black solid structure histograms of Pollena particles and green histogram of Avellino particles; Figure 3);
- poorly vesiculated particle with tubular vesicles (Agnano Monte Spina particles, Figure 2 and light blue histogram of Figure 3) or;

- highly vesiculated particle with a portion of poorly vesiculated glass (Agnano Monte Spina particles, Figure 2; orange histogram of Figure 3).

Eyjafjallajökull and Etna particles show coarser vesicles than Avellino, Pollena and Agnano Monte Spina particles, and display a wide range of solid structure size (Figures 2, 3). However, Eyjafjallajökull particles have smaller structure thickness values than those of Etna, except for three particles, which have a thick solid structure due to the presence of large phenocrysts (Figure 2). In general, for Etna particles, the thick solid structure is mainly related to a higher content of large phenocrystals than Eyjafjallajökull particles (Figure 2). Grímsvötn particles show the largest range of vesicle size with a thick solid structure, which is mainly represented by glass (Figure 2).

It was also observed that the solid structure is well correlated with particle vesicularity (Figure 4); in particular, the thinner the solid structure, the greater the particle vesicularity. This behavior is further corroborated by the significant correlation between structure linear density of vesicles and vesicularity (Figure 4), i.e. the distance between vesicles decreases (i.e. the structure linear density value increases) with increasing particle vesicularity. The latter show also a negative correlation with the surface convexity index, i.e. vesicularity increases as surface convexity index decreases, meaning that vesicles are better inter-connected (Figure 4).

Concerning the influence of internal texture on particle shape, Figure 5 shows that with increasing vesicularity, Φ_{3D} decreases and D_{3D} increases, i.e. particles are more irregular. Furthermore, a particle's irregularity increases with decreasing thickness of the solid structure, hence decreasing the distance between vesicles and with increasing inter-connection of vesicles (Figure 5). It is notable that particle shape is well-constrained by a thorough analysis of all parameters related to the internal structure. For example, Avellino particles tend to be more irregular than Agnano Monte Spina particles, despite having a similar vesicle and solid structure distribution (Figure 3) and the same vesicularity range (Figure 5). This difference of shape can instead be attributed to a higher inter-connectivity and lower distance between vesicles of Avellino particles than Agnano Monte Spina particles (Figure 5).

In addition, results suggest how particles produced by magma of the same composition and by similar fragmentation processes (Group 1 and 2 above) might not display similar shape parameters. For example, Avellino and Pollena particles have different shapes (Table 2, Figure 5) that can be related to both a different vesiculation and crystallization history as shown by the vesicularity, surface convexity index, solid structure thickness and structure linear density parameters (Figure 5). Furthermore, these particles display the same vesicle size (Figures 2, 3) but Pollena particles are less vesiculated with a poor inter-connectivity of vesicles than Avellino particles (Figure 5). Finally, Pollena particles have a thicker solid structure, which is reflected in a greater distance between vesicles (Figures 4, 5), caused by both a greater thickness of the glass and a greater presence of phenocrysts (Fig. 6).

4. CONCLUSIONS

The use of μX-CT has allowed us to demonstrate that particle shape, which is here described by sphericity Φ_{3D} and fractal dimension D_{3D}, is strongly influenced by the internal structure of particles, here quantified by means of vesicularity, vesicle and solid structure distribution, vesicle inter-connectivity and distance between adjacent vesicles. These textural features have been found to vary with magma composition and show that volcanic particles collected from tephra fallout deposits of eruptions of different magnitudes, styles and magma composition show different shapes.

This work highlights that, for modelling purposes, the assumption that particles of different eruptions, which are produced by magma of the same composition and by similar fragmentation processes, have the same shape, might not be correct. Therefore, it is necessary to obtain particle shape for each case study.

Furthermore, our results confirm that μX-CT is a powerful tool for investigating the shape and internal structure of particles. It both allows us to characterize the shape of irregular particles by means of tridimensional shape parameters and to relate them to the internal structures of particles.

Acknowledgments

Brucker Skyscan 1172 high-resolution μX –CT scanner has been purchased with funds from "PON Ricerca e Competitività 2007-2013".

Published with permission of the Executive Director of British Geological Survey (UKRI).

We thank the Editor Mattia de' Michieli Vitturi, Margherita Pollacci and an anonymous reviewer for improving the early version of the manuscript.

We finally thank Susan C. Loughlin for her comments and suggestions.

REFERENCES

Arzilli, F., M. Polacci, P. Landi, D. Giordano, D.R. Baker and L. Mancini (2016). A novel protocol for resolving feldspar crystals in synchrotron X-ray microtomographic images of crystallized natural magmas and synthetic analogs. American Mineralogist,101, 2301-2311.

Bagheri, G.H., C. Bonadonna, I. Manzella and P. Vonlanthen (2015). On the characterization of size and shape of irregular particles. Powder Technology, 270, 141–153. https://doi.org/10.1016/j.powtec.2014.10.015.

Bagheri, G.H. and C. Bonadonna (2016). On the drag of freely falling non-spherical particles. Powder Technology, 301, 526–544. http://dx.doi.org/10.1016/j.powtec.2016.06.015.

Baker, D.R., L. Mancini, M. Polacci, M.D. Higgins, G.A.R. Gualda, R.J. Hill and M. Rivers (2012). An introduction to the application of X-ray microtomography to the three-dimensional study of igneous rocks. Lithos, 148, 262–276.

Beckett, F.M., C.S. Witham, M.C. Hort, J.A. Stevenson, C. Bonadonna and S.C. Millington (2015). Sensitivity of dispersion model forecasts of volcanic ash clouds to the physical characteristics of the particles. Journal of Geophysical Research Atmospheres, 120, 11636–11652. https://doi. org/10.1002/2015JD023609.

Blong, R.J. (1984). Volcanic Hazards. A Sourcebook on the Effects of Eruptions. Academic Press, Sidney, Australia.

Bonadonna, C., A. Folch, S. Loughlin and H. Puempel (2012). Future developments in modeling and monitoring of volcanic ash clouds: outcomes from the first IAVCEI-WMO workshop on ash dispersal forecast and civil aviation. Bulletin of Volcanology, 74, 1–10. https://doi.org/10.1007/s00445-011-0508-6.

Branney, M.J. and P. Kokelaar (2002). Pyroclastic density currents and the sedimentation of ignimbrites. Geological Society, London, Memoirs, 27

Casadevall, T.J. (1994). The 1989–1990 eruption of Redoubt Volcano, Alaska: impacts on aircraft operations. Journal of Volcanology and Geothermal Research, 62, 301–316.

Chappard, D., E. Legrand, B. Haettich, G. Chales, B. Auvinet, J.P. Eschard, J.P. Hamelin, M.F. Basle and M. Audran (2001). Fractal dimension of trabecular bone: comparison of three histomorphometric computed techniques for measuring the architectural two-dimensional complexity. Journal of Pathology, 195, 515–521. http://dx.doi.org/10.1002/path.970.

Chien, S.F. (1994). Settling velocity of irregularly shaped particles. SPE Drilling & Completion, 9, 281–288.

Cnudde, V. and M.N. Boone (2013). High-resolution X-ray computed tomography in geosciences: A review of the current technology and applications. Earth-Science Reviews, 123, 1-17.

de Vita, S., G. Orsi, L. Civetta, A. Carandente, M. D'Antonio, T. Di Cesare, M.A. Di Vito, R.V. Fisher, R. Isaia, E. Marotta, M. Ort, L. Pappalardo and J. Southon (1999). The Agnano-Monte Spina eruption in the densely populated, restless Campi Flegrei caldera (Italy). Journal of Volcanology and Geothermal Research, 91, 269–301.

Dellino, P., R. Isaia, L. La Volpe and G. Orsi (2001). Statistical analysis of textural data from complex pyroclastic sequence: implication for fragmentation processes of the Agnano-Monte Spina eruption (4.1 ka), Phlegraean Fields, southern Italy. Bulletin of Volcanology, 63, 443–461.

Dellino, P., D. Mele, R. Bonasia, G. Braia, L. La Volpe and R. Sulpizio (2005). The analysis of the influence of pumice shape on its terminal velocity. Geophysical Research Letters 32, L21306. https://doi.org/10.1029/2005GL023954.

Dellino, P., M.T. Gudmundsson, G. Larsen, D. Mele, J.A. Stevenson, T. Thordarson and B. Zimanowski (2012). Ash from the Eyjafjallajökull eruption (Iceland): fragmentation processes and aerodynamic behavior. Journal of Geophysical Research, 117, B00C04.

http://dx.doi.org/10.1029/2011JB008726.s

Dellino, P., F. Dioguardi, D.M. Doronzo and D. Mele (2018). The rate of sedimentation from turbulent suspension: an experimental model with application to pyroclastic density currents and discussion on the grain-size dependence of flow runout. Sedimentology, in press. https://doi.org/10.1111/sed.12485

Dioguardi, F., P. Dellino and D. Mele (2014). Integration of a new shape-dependent particle–fluid drag coefficient law in the multiphase Eulerian–Lagrangian code MFIX-DEM. Powder Technology, 260, 68–77. http://dx.doi.org/10.1016/j.powtec.2014.03.071.

Dioguardi, F. and P. Dellino (2014). PYFLOW: a computer code for the calculation of the impact parameters of dilute pyroclastic density currents (DPDC) based on field data. Computers & Geosciences 66:200–210. http://dx.doi.org/10.1016/j.cageo.2014.01.013.

Dioguardi, F. and Mele D. (2015). A new shape dependent drag correlation formula for non-spherical rough particles. Experiments and results. Powder Technology, 277, 222–230. http://dx.doi.org/10.1016/j.powtec.2015.02.062.

Dioguardi, F., D. Mele, P. Dellino and T. Dürig (2017). The terminal velocity of volcanic particles with shape obtained from 3D X-ray microtomography. Journal of Volcanology and Geothermal Research, 329, 41–53.

Dioguardi, F. and D. Mele (2018). PYFLOW_2.0: a computer program for calculating flow properties and impact parameters of past dilute pyroclastic density currents based on field data. Bulletin of Volcanology, 80, 28. doi.org/10.1007/s00445-017-1191-z.

Dioguardi F., D. Mele and P. Dellino (2018). A new one-equation model of fluid drag for irregularly-shaped particles valid over a wide range of Reynolds number. Journal of Geophysical Research, 123(1), 144-156. doi:10.1002/2017JB014926.

Doronzo, D.M., E.A. Khalaf, P. Dellino, M.D. de Tullio, F. Dioguardi, F., L. Gurioli, D. Mele, G. Pascazio and R. Sulpizio (2015). Local impact of dust storms around a suburban building in arid and semi-arid regions: numerical simulation examples from Dubai and Riyadh, Arabian Peninsula. Arabian Journal of Geosciences, 8, 7359. http://dx.doi.org/10.1007/s12517- 014-1730-2.

Dufek, J. (2016). The fluid mechanics of pyroclastic density currents. Annual Review of Fluid Mechanics, 48(1), 459–485. https://doi.org/10.1146/annurevfluid-122414-034252

Ersoy, O., E. Şen, E. Aydar, İ. Tatar and H.H. Çelik, (2010). Surface area and volume measurements of volcanic ash particles using micro-computed tomography (micro-CT): a comparison with scanning electron microscope (SEM) stereoscopic imaging and geometric considerations. Journal of Volcanology and Geothermal Research, 196, 281–286.

Feldkamp, L.A., L.C. Davis and J.W. Kress (1984). Practical cone-beam algorithm. Journal of the Optical Society of America, A 1, 612–619.

Ganser, G.H. (1993). A rotational approach to drag prediction of spherical and non-spherical particles. Powder Technology, 77, 143–152. https://doi.org/10.1016/0032-5910(93)80051-B.

Haider, A. and O. Levenspiel (1989). Drag coefficient and terminal velocity of spherical and non-spherical particles. Powder Technology, 58, 63–70. https://doi.org/10.1016/0032-5910(89)80008-7.

Hahn, M., M. Vogel, M. Pompesius-Kempa and G. Delling (1992). Trabecular bone pattern factor – a new parameter for simple quantification of bone microarchitecture. Bone, 13, 327-330.

Hildebrand, T., A. Laib, R. Müller, J. Dequeker and P. Rüegsegger (1999). Direct three-dimensional morphometric analysis of human cancellous bone: Microstructural data from spine, femur, iliac crest, and calcaneus. Journal of Bone and Mineral Research, 14(7), 1167-1174. doi:10.1359/jbmr.1999.14.7.1167.

Hölzer, A. and M. Sommerfeld (2008). New simple correlation formula for the drag coefficient of non-spherical particles. Powder Technology, 184, 361–365. http://dx.doi.org/10.1016/j.powtec.2007.08.021.

Horwell, C.J. and P.J. Baxter (2006). The respiratory health hazards of volcanic ash: a review for volcanic risk mitigation. Bulletin of Volcanology, 69, 1–24.

Jones, A.R., D.J. Thomson, M. Hort and B. Devenish (2007). The U.K. Met Office's next-generation atmospheric dispersion model, NAME III, in Borrego C. and Norman A.-L. (Eds) Air Pollution Modeling and its Application XVII (Proceedings of the 27th NATO/CCMS International Technical Meeting on Air Pollution Modelling and its Application), Springer, pp. 580-589, 2007.

Jude-Eton, T.C., T. Thordarson and B. Oddsson (2012). Dynamics, stratigraphy and proximal dispersal of supraglacial tephra during the ice-confined 2004 eruption at Grímsvötn volcano, Iceland. Bulletin of Volcanology, 74 (5), 1057–1082.

Kok, J.F., E.J.R. Parteli, T.I. Michaels and D.B. Karam DB (2012). The physics of wind-blown sand and dust. Reports on Progress in Physics, 75, 1–72.

Liu, X. and A. Sasov (2005). Cluster reconstruction strategies for microCT/nanoCTscanners. Proceedings of Fully 3D Image Reconstruction Meeting in Radiology and Nuclear Medicine, Salt Lake City (USA)

Lorensen, W.E. and H.E. Cline (1987). Marching cubes: a high resolution 3D surface construction algorithm. Computers & Grapics, 21(4), 163–169.

Loth, E. (2008). Drag of non-spherical solid particles of regular and irregular shape. Powder Technology, 182, 342–353.

Mastin, L. G., M. Randall, J.H. Schwaiger and R. Denlinger (2013). User's Guide and Reference to Ash3d: A Three-Dimensional Model for Atmospheric Tephra Transport and Deposition. U.S. Geological Survey Open-File Report, 2013-1122, 48 pp.

Mele, D., P. Dellino, R. Sulpizio and G. Braia (2011). A systematic investigation on the aerodynamics of ash particles. Journal of Volcanology and Geothermal Research, 203 (1),1–11. http://dx.doi.org/10.1016/j.jvolgeores.2011.04.004.

Mele, D., F. Dioguardi, P. Dellino, R. Isaia, R. Sulpizio and G. Braia G (2015). Hazard of pyroclastic density currents at the Campi Flegrei Caldera (Southern Italy) as deduced from the combined use of facies architecture, physical modeling and statistics of the impact parameters. Journal of Volcanology and Geothermal Research, 299, 35–53. https://doi.org/10.1016/j.jvolgeores.2015.04.002

Mele, D. and F. Dioguardi (2018). The grain size dependency of vesicular particle shapes strongly affects the drag of particles. First results from microtomography investigations of Campi Flegrei fallout deposits. Journal of Volcanology and Geothermal Research, 353, 18-24. doi:10.1016/j.jvolgeores.2018.01.023.

Otsu, N. (1979). A threshold selection method from gray-level histograms. IEEE Transactions on Systems, Man, and Cybernetics, 9(1), 62–66. https://doi.org/10.1109/TSMC.1979.4310076.

Pfeiffer, T., A. Costa and G. Macedonio (2005). A model for the numerical simulation of tephra fall deposits. Journal of Volcanology and Geothermal Research, 140, 273–294. https://doi.org/10.1016/j.jvolgeores.2004.09.001.

Polacci, M., F. Arzilli, G. La Spina, N. Le Gall, B. Cai, M.E. Hartley, D. Di Genova, N.T. Vo, S. Nonni, R.C. Atwood, E.W. Llewellin, P.D. Lee and M.R. Burton (2018). Crystallisation in basaltic magmas revealed via in situ 4D synchrotron X-ray microtomography. Scientific Reports, 8(1), 8377.

Promentilla, M.A.B., T. Sugiyama, T. Hitomi and N. Takeda (2009). Quantification of tortuosity in hardened cement pastes using synchrotron-based X-ray computed microtomography. Cement and Concrete Research, 39, 548–557.

Rausch, J., B. Grobéty and P. Volanthen (2015). Eifel maars: quantitative shape characterization of juvenile ash particles (Eifel Volcanic Field, Germany). Journal of Volcanology and Geothermal Research, 291, 86–100. https://doi.org/10.1016/j.jvolgeores.2014.11.008.

Remy, E. and E. Thiel (2002). Medial axis for chamfer distances: computing look-up tables and neighborhoods in 2D or 3D. Pattern Recognition Letters, 23(6), 649–661.

Rodrigue, D., D. DeKee and R.P. Chhabra (1994). Drag on non-spherical particles in non-Newtonian fluids. The Canadian Journal of Chemical Engineering 72, 588–593.

Scollo, S., P. Del Carlo and M. Coltelli (2007). Tephra fallout of 2001 Etna flank eruption: analysis of the deposit and plume dispersion. Journal of Volcanology and Geothermal Research,160, 147-164.

SKYSCAN, Structural parameters measured by SkyScan CT-analyser software. August 1, 2009.

Sneed, E. and R. Folk (1958). Pebbles in the lower Colorado River, Texas a study in particle morphogenesis. The Journal of Geology, 66(2), 114–150.

Song, S.R., K.W. Jones, W.B. Lindquist, B.A. Dowd and D.L. Sahagian (2001). Synchrotron X-ray computed microtomography: studies on vesiculated basaltic rocks. Bulletin of Volcanology, 63, 252–263. http://dx.doi.org/10.1007/s004450100141.

Sulpizio, R., D. Mele, P. Dellino and L. La Volpe (2005). A complex, subplinian-type eruption from low-viscosity, tephri-phonolitic magma: the Pollena eruption of Somma-Vesuvius (Italy). Bulletin of Volcanology, 67, 743–767.

Sulpizio, R., R. Cioni, M.A. Di Vito, D. Mele, R. Bonasia, P. Dellino and L. La Volpe (2010). The Pomici di Avellino eruption of Somma-Vesuvius (3.9 ka BP) part I: stratigraphy, compositional variably and eruptive dynamics. Bulletin of Volcanology, 72, 539–558. http://dx.doi.org/10.1007/s00445-009-0339-x.

Swamee, P.K. and C.P. Ojha (1991). Drag coefficient and fall velocity of non spherical particles. Journal of Hydraulic Engineering, 117, 660–669. https://doi.org/10.1061/(ASCE)0733-9429(1991)117:5 (660).

Taylor, M. (2002). Quantitative measures for shape and size of particles. Powder Technology, 124, 94–100.

Tran-Cong, S., M. Gay and E.E. Michaelides (2004). Drag coefficients of irregularly shaped particles. Powder Technology, 139, 21–32. https://doi.org/10.1016/j.powtec.2003.

Voltolini, M., D. Zandomeneghi, L. Mancini and M. Polacci (2011). Texture analysis of volcanic rock samples: quantitative study of crystals and vesicles shape preferred orientation from X-ray microtomography data. Journal of Volcanology and Geothermal Research, 202, 83–95.

Vonlanthen, P., J. Rausch, R.A. Ketcham, B. Putlitz, L.P. Baumgartner and B. Grobéty (2015). High-resolution 3D analyses of the shape and internal constituents of small volcanic ash particles: the contribution of SEMmicro-computed tomography (SEMmicro-CT). Journal of Volcanology and Geothermal Research, 293, 1–12. https://doi.org/10.1016/j.jvolgeores.2014.11.016.

Wilson, L. and T. Huang (1979). The influence of shape on the atmospheric settling velocity of volcanic ash particles. Earth and Planetary Science Letters, 44, 311–324.

Wilson, T.M., C. Stewart, V. Sword-Daniels, G.S. Leonard, D.M. Johnston, J.W. Cole, J.B. Wardman, G. Wilson and S.T. Barnard (2012). Volcanic ash impacts on critical infrastructure. Physics and Chemistry of the Earth, 45–46, 5–23.

Wilson, G., T.M. Wilson, N.I. Deligne and J.W. Cole (2014). Volcanic hazard impacts to critical infrastructure: a review. Journal of Volcanology and Geothermal Research, 286(1), 148–182.

Tables

μX-CT scanner parameters		**Reconstruction parameters**	
Pixel Size (μm)	1.02	Smoothing	1
X-ray Voltage (kV)	48	Ring Artifact correction	6
X-ray Current (μA)	208	Beam Hardening Correction (%)	56
Rotation Step (degrees)	0.37	-	

Filter	No filter	-
Frame averaging	5	-

Table 1. Scan parameters of the μX-CT scanner and cross-section reconstruction.

	unit	Eyjafjallajökull	Grímsvötn	Etna	Avellino	Agnano M. Spina	Pollena
Object volume	mm^3	0.041±0.014	0.039±0.013	0.041±0.009	0.035±0.011	0.041±0.021	0.047±0.010
Vesicularity	%	23.8±11.9	16.0±6.4	16.2±9.5	48.0±9.9	39.3±14.0	24.9±7,6
Solid structure size	mm	0.052±0.024	0.062±0.024	0.069±0.032	0.016±0.011	0.019±0.010	0.027±0.017
Vesicle size	mm	0.029±0.016	0.042±0.021	0.029±0.017	0.018±0.010	0.017±0.010	0.018±0.011
Surface convexity index	1/mm	107.5±28.7	104.2±16.8	133.5±35.2	31.8±46.6	93.6±64.0	167.6±47.2
Structure linear density	1/mm	8.38±4.71	4.31±2.62	5.64±2.97	27.35±3.51	21.96±5.49	14.40±4.96
D_{3D}	-	2.288±0.095	2.165±0.058	2.230±0.093	2.564±0.057	2.445±0.154	2.288±0.141
Φ_{3D}	-	0.244±0.096	0.383±0.075	0.314±0.102	0.073±0.040	0.151±0.134	0.316±0.139

Table 2. Average values and standard deviations of 3D parameters of all analyzed particles.

Figure Captions

Figure 1. Two examples of segmentation and creation of VOI (Volume of interest) by means of shrink-wrap operation. a, b and c: raw, binary and ROI (Region of Interest) images of one cross section of a Grímsvötn particle. d, e and f: raw, binary and ROI (Region of Interest) images of one cross section of a Agnano Monte Spina particle.

Figure 2. Solid structure size vs. vesicle size diagram. 3D surface rendering and cross section images of few particles are also insert. The red line inside the reconstructed particles indicates the position of the displayed cross section image.

Figure 3. Vesicle and solid structure distribution histograms of all analyzed particles.

Figure 4. Structure linear density, solid structure size and surface convexity index vs. vesicularity diagrams of all analyzed particles. -

Figure 5. Sphericity Φ_{3D} and fractal dimension D_{3D} vs. vesicularity, surface convexity index, solid structure size and structure linear density diagrams of all analyzed particles.

Figure 6. 3D surface rendering (with Maximum intensity projection function) and cross section image of two particles of Avellino and Pollena eruption. The red line inside the reconstructed particles indicates the position of the displayed cross section image.

Figure 1

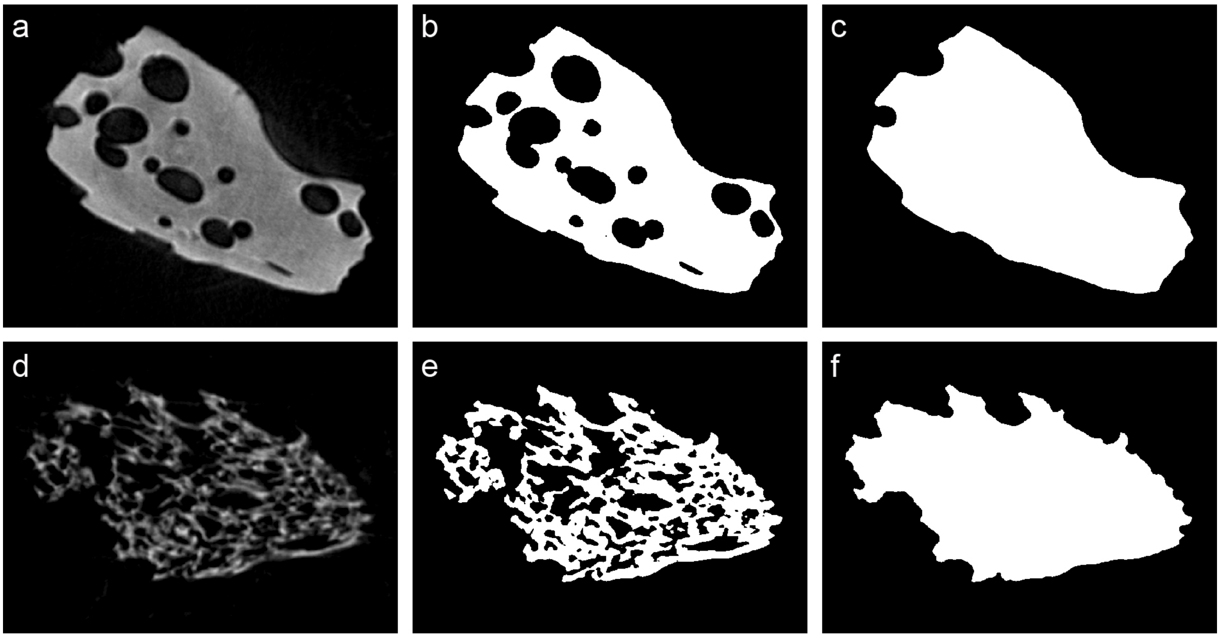

Figure 2

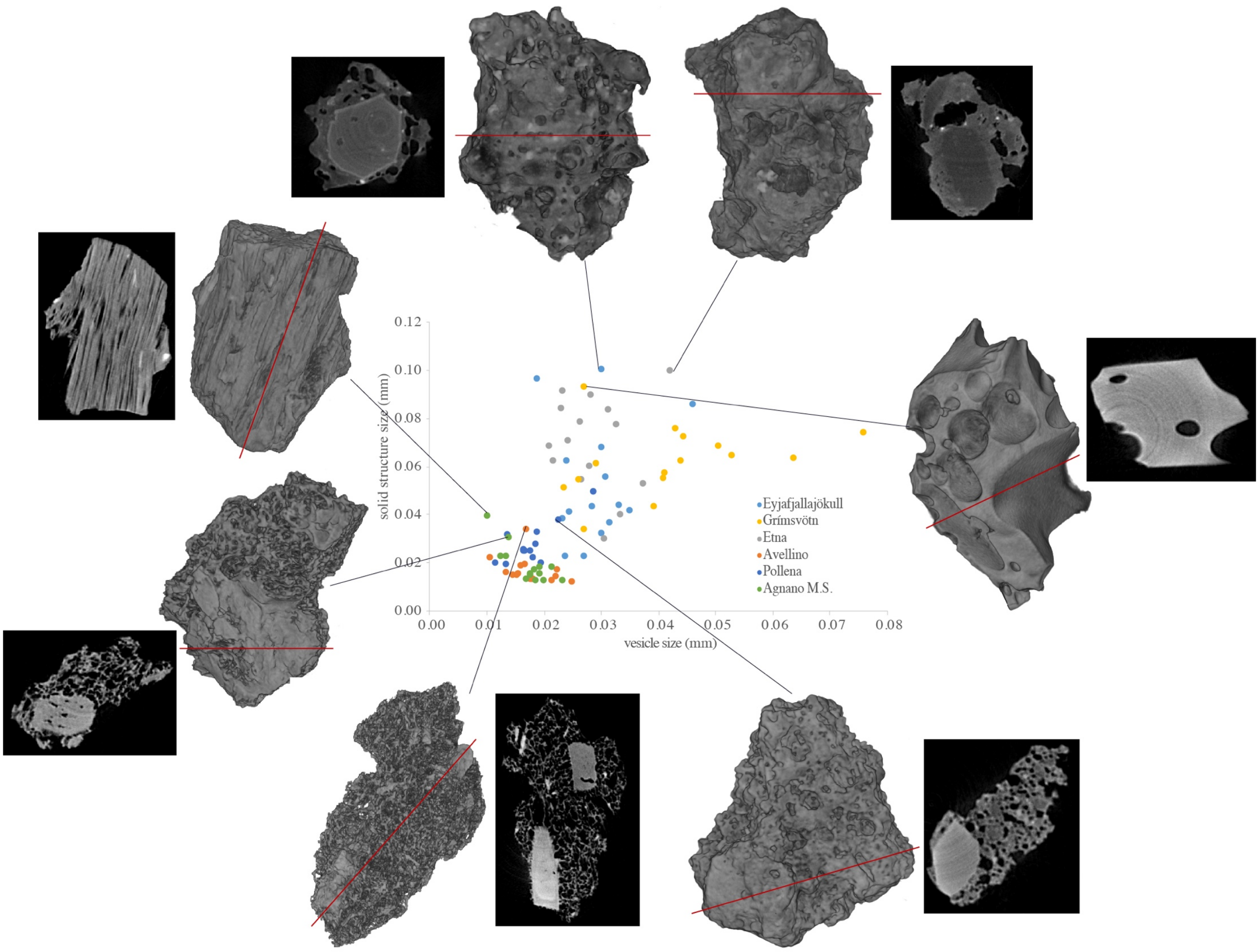

Figure 3

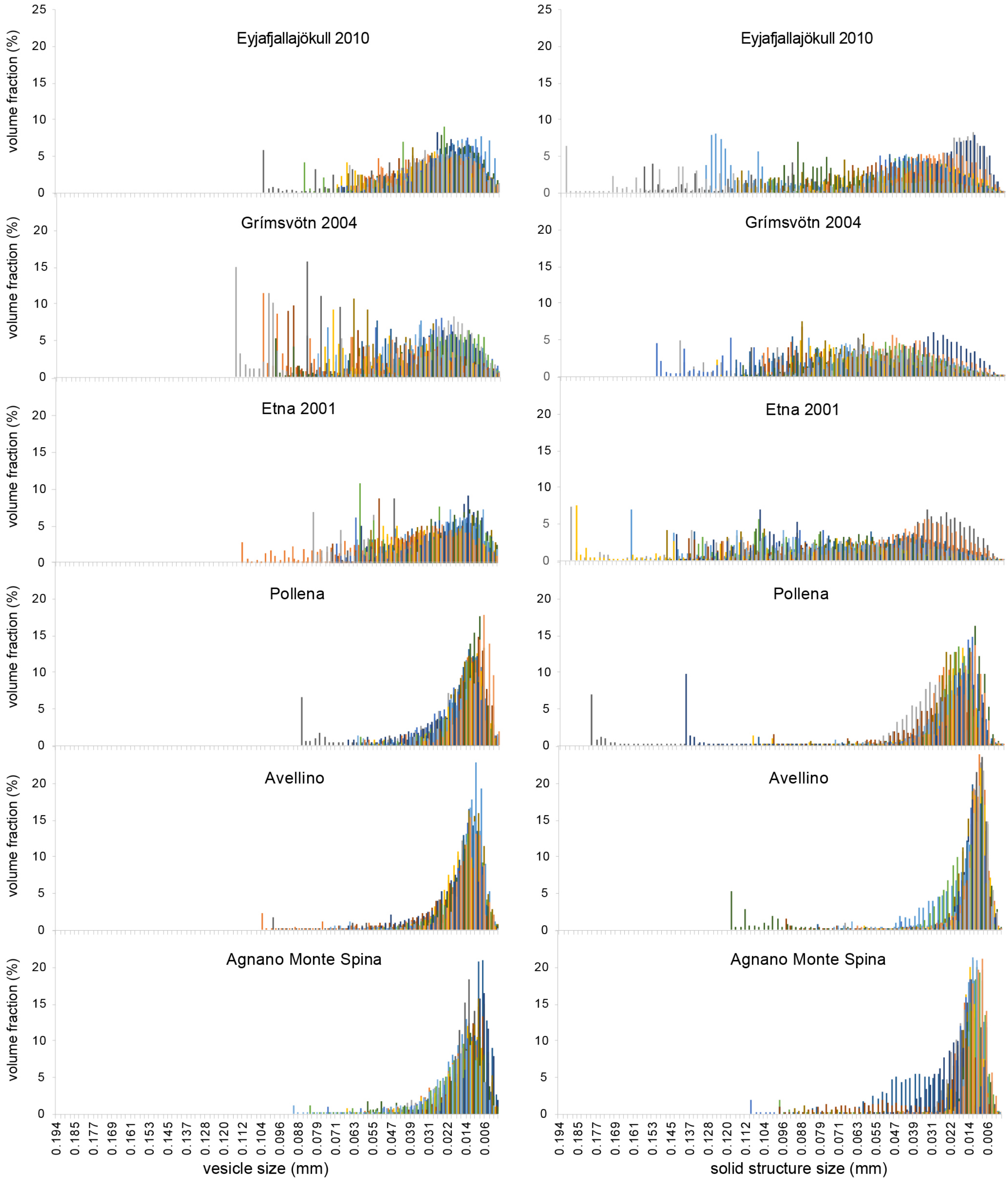
Eyjafjallajökull 2010
Eyjafjallajökull 2010
Grímsvötn 2004
Grímsvötn 2004
Etna 2001
Etna 2001
Pollena
Pollena
Avellino
Avellino
Agnano Monte Spina
Agnano Monte Spina
volume fraction (%)
0.194 0.185 0.177 0.169 0.161 0.153 0.145 0.137 0.128 0.120 0.112 0.104 0.096 0.088 0.079 0.071 0.063 0.055 0.047 0.039 0.031 0.022 0.014 0.006
vesicle size (mm)
solid structure size (mm)

Figure 4

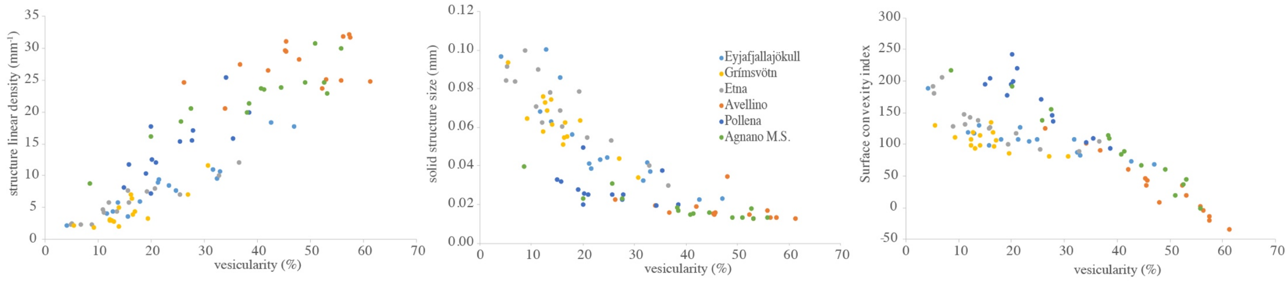

Figure 5

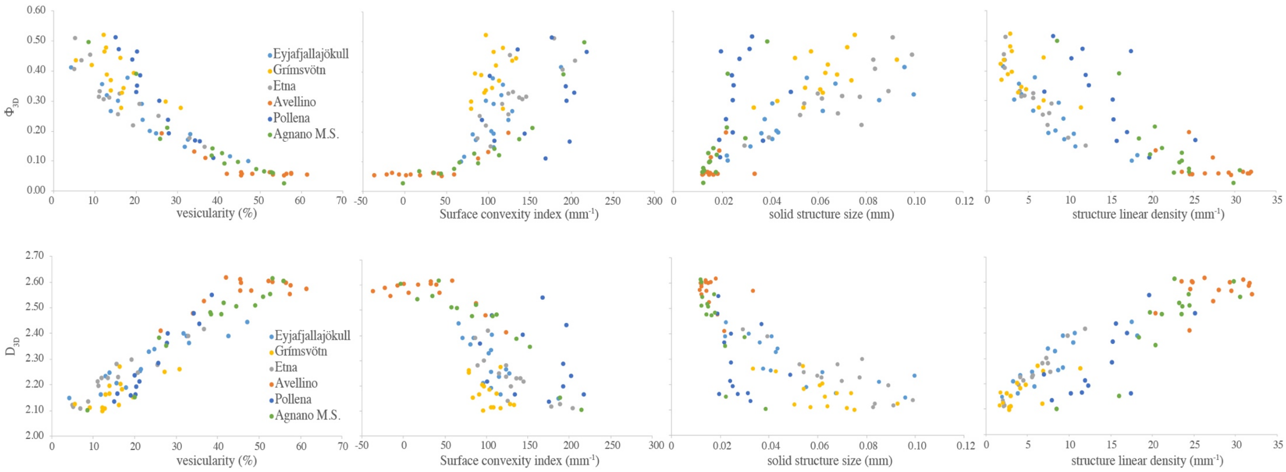

Figure 6